TWO-SCALE MODEL FOR THE EVALUATION OF SEA-SURFACE SCATTERING IN GNSS-R SHIP-DETECTION APPLICATIONS

Maurizio Di Bisceglie[1], Gerardo Di Martino[2], Alessio Di Simone[2], Carmela Galdi[1], Antonio Iodice[2], Daniele Riccio[2], Giuseppe Ruello[2]

[1]Università del Sannio, Benevento, Italy. [2]Università di Napoli Federico II, Naples, Italy

ABSTRACT

Ocean GNSS-R is successfully being employed to retrieve wind speed from GNSS signals scattered by the sea surface. To obtain a sufficient scattered field intensity from the ocean surface, the receiver acquires data when it is located along the specular reflection direction. However, new applications of GNSS-R are being explored, among which ship-detection. In this case, scattering from the ocean represents the clutter to be suppressed, so that a different geometry, where the GNSS signals are received in backscattering configuration, is preferable to the forward scattering one. In this new geometry, the Geometric Optics, usually employed in the GNSS-R scientific community, is often no more appropriate to model scattering from the sea surface, and different scattering models must be used. To this aim, we here introduce the Polarimetric Two-Scale Model to evaluate the intensity of the GNSS backscattered signal.

Index Terms— GNSS-R, sea surface scattering, two-scale model, ship detection.

1. INTRODUCTION

In ocean Global Navigation Satellite System Reflectometry (GNSS-R) the transmitted signal, reflected in the specular direction by the ocean surface, is captured by a receiver and processed to obtain information about the sensed surface. Retrieval of wind speed represents the main product of such technique [1,2]. The signals of opportunity contain the ocean electromagnetic scattering properties and new applications have been explored to fully exploit such information that is gathered by satellite sensors in almost any time and space. In this study we consider a different geometry where the GNSS signals are received in backscattering configuration rather that in forward scattering, with the final purpose of detecting objects on the sea surface. The backscattering configuration appears more suitable for approaching such problem because the ocean radar cross section (RCS) is quite low for such geometry, compared to the forward scattering configuration. There are few studies related to this problem. In [3] a first analysis demonstrates some advantages of backscattering geometry with respect to forward scattering. More recent investigations can be found in [4,5,6] where several detection

strategies are assessed. The main conclusions of the previous studies are that the forward scattering returns from the sea surface and the resolution limits determined by the transmitted PRN sequence do not allow detection of targets with radar cross section corresponding to normal-size ships. Therefore, in this paper we analyze the detection performance by assuming that the target lies in the subspace in front of the receiver in the backscattering direction. We here focus on the sea clutter electromagnetic modelling: in fact, while for scattering directions not far from the specular one the Kirchhoff Approximation in the Geometric Optics (KAGO) allows to accurately evaluate the field scattered by the sea surface, this is not the case if the scattering direction is far from the specular one. This happens in the backscattering configuration if the considered GNSS transmitting satellite is not at near nadir. In the latter case, also the Bragg scattering component must be considered. To this aim, here it is assumed that the sea surface can be described using the two-scale model (see, e.g., [7]) with wind-driven waves with power–law spectrum decay [8-10]. The closed-form analytical backscattering solution provided in [11-12] is here reformulated to adapt it to the circularly polarized signal radiated by GNSS transmitters.

2. TWO-SCALE MODEL DEVELOPMENT

The scattering model is based on a two-scale description of the sea surface, i.e. large-scale variations with small-scale roughness superimposed. The large scale-roughness is approximated using rough facets, large with respect to the wavelength and small with respect to sensor resolution. Accordingly, the surface height of a facet, as a function of azimuth x and range y, can be described as

$$z(x, y) = a(x - x_i) + b(y - y_i) + z_i + \delta(x, y) \qquad (1)$$

where x and y are GNSS-R reference coordinates, a and b are the local slopes along x and y, respectively; x_i, y_i, and z_i are the coordinates of the ith facet center; $\delta(x, y)$ accounts for the small-scale roughness.

Large-scale and small-scale roughness are modeled as independent stochastic processes. In particular, azimuth and range slopes are independent identically distributed zero-mean σ^2-variance Gaussian random variables, i.e., a, $b \sim$

$N(0,\sigma^2)$. With regard to the small-scale roughness, it is of key importance to select a model able to adequately describe the sea surface roughness at the microwave frequencies of interest. In particular, from the viewpoint of scattering evaluation we need an expression for the power spectral density (PSD) of the sea surface. Several expressions of the sea spectrum are available in the literature [8-10]: among them the Elfouhaily omnidirectional spectrum provides an accurate description for the case of partially developed sea [8]. We are interested here in the spectrum at the Bragg resonant wavenumber $\kappa = 2k \sin\theta_l$, where $k = 2\pi/\lambda$ is the electromagnetic wavenumber, λ is the electromagnetic wavelength, and θ_l is the local incidence angle of the facet. The value of κ in L-band for intermediate values of the incidence angle corresponds to wavenumbers between 15 and 35 m^{-1}. It can be shown that in this region Elfouhaily spectrum presents a power-law fractal behavior with a *Hurst parameter* H_t=0.75, and that its behavior as a function of the local wind is the same of the modified Pierson-Moskowitz omnidirectional spectrum [10], apart from a proportionality constant. For this reason, without loss of generality, we here use the modified Pierson-Moskowitz spectrum, since its expression is simpler than the Elfouhaily one. Therefore, we use the following one-dimensional omnidirectional PSD:

$$W(\kappa) = \frac{Bu_*}{\kappa^{1+2H_t}} = \frac{Bu_*}{\kappa^{2.5}} \tag{2}$$

where B [s/m$^{1/2}$] is a dimensional constant and u_* is the friction velocity. The two-dimensional spectrum can be obtained from the omnidirectional one using the following relation:

$$W(\kappa_x, \kappa_y) = \frac{1}{\kappa} W(\kappa) f(\kappa,\phi) = u_* W_n(\kappa_x, \kappa_y) \tag{3}$$

where $f(\kappa,\phi)$ is the angular spreading function, ϕ is the wave direction relative to the wind, $\kappa_x = \kappa\cos\phi$, $\kappa_y = \kappa\sin\phi$, and W_n is the wind-independent part of the directional spectrum. Note that in the range of wavenumbers of interest f is practically constant with κ and only weakly dependent on u_* [8-9]: in this paper we are neglecting both these dependencies.

We now face the problem of scattering evaluation: here we focus on the backscattering case. The overall Normalized Radar Cross Section (NRCS) is given by the sum of two contributions: the specular contribution, arising from the usual KAGO formulation [9,11], and the Bragg contribution, that can be computed by using the Polarimetric-Two-Scale Model (PTSM) [11-12], that we reformulate in the following to adapt it to the circular polarization case. The geometry of the problem is illustrated in Fig. 1. The facet random tilt gives rise to a random rotation β of the local incidence plane and to a drift of the local incidence angle θ_l, where β and θ_l can be expressed as functions of the global incidence angle θ, of x-slope a, and y-slope b [11]. The PTSM takes into account both these effects. In particular, the elements of the scattering

matrix of the randomly-tilted randomly-rough facet can be evaluated using the first-order Small-Perturbation Method (SPM) and can be expressed as follows:

$$S_{pq} = \frac{k^2 \cos^2\theta_l}{\pi} \chi_{pq}(\theta_l,\beta) \tilde{\delta}(0, 2k\sin\theta_l) \tag{4}$$

where $\tilde{\delta}(k_x, k_y)$ is the Fourier transform of $\delta(x,y)$, p and q are the polarizations of incident and scattered fields, respectively; χ_{pq} are the elements of the matrix

$$\underline{\underline{\chi}}(\theta_l,\beta) = \underline{\underline{R_2}}(\beta) \cdot \begin{pmatrix} F_H(\theta_l,\varepsilon) & 0 \\ 0 & F_V(\theta_l,\varepsilon) \end{pmatrix} \cdot \underline{\underline{R_2^{-1}}}(\beta) \tag{5}$$

wherein

$$\underline{\underline{R_2}}(\beta) = \begin{pmatrix} \cos\beta & \sin\beta \\ -\sin\beta & \cos\beta \end{pmatrix} \tag{6}$$

is the unitary rotation matrix, and F_H and F_V are the Bragg coefficients for horizontal and vertical polarization, respectively [9,11], depending on the sea water relative permittivity ε. Therefore, the entries of the covariance matrix of the single facet can be written as follows:

$$\langle S_{pq} S_{rs}^* \rangle_\delta = \frac{A k^4 \cos^4\theta_l}{\pi^2} \chi_{pq}(\theta_l,\beta) \chi_{rs}^*(\theta_l,\beta) W(0, 2k\sin\theta_l) \tag{7}$$

wherein $\langle\cdot\rangle_\delta$ stands for statistical mean with respect to the random variable δ and A is the area of the facet projected on the azimuth-ground range plane. In the hypothesis that the returns from the facets can be considered uncorrelated and for small values of the facets' slope, the covariance matrix of the whole surface can be obtained from the one of the single facet averaging over the surface slopes a and b, after a second-order expansion around a=0 and b=0. In particular, the following expressions are obtained [11-12]:

$$\begin{cases} \langle |S_{hh}|^2 \rangle_{\delta,a,b} = C_{0,0}^{hh} + \left(C_{2,0}^{hh} + C_{0,2}^{hh} + 2\frac{\mathrm{Re}\{C_{0,0}^{hv}\}-C_{0,0}^{hh}}{\sin^2\theta} \right)\sigma^2 \\ \langle |S_{vv}|^2 \rangle_{\delta,a,b} = C_{0,0}^{vv} + \left(C_{2,0}^{vv} + C_{0,2}^{vv} + 2\frac{\mathrm{Re}\{C_{0,0}^{hv}\}-C_{0,0}^{vv}}{\sin^2\theta} \right)\sigma^2 \\ \langle S_{hh} S_{vv}^* \rangle_{\delta,a,b} = C_{0,0}^{hv} + \left(C_{2,0}^{hv} + C_{0,2}^{hv} + 2\frac{C_{0,0}^{hh}+C_{0,0}^{vv}-2C_{0,0}^{hv}}{\sin^2\theta} \right)\sigma^2 \\ \langle |S_{hv}|^2 \rangle_{\delta,a,b} = \left(C_{0,0}^{hh} + C_{0,0}^{vv} - 2\mathrm{Re}\{C_{0,0}^{hv}\} \right)\frac{\sigma^2}{\sin^2\theta} \end{cases} \tag{8}$$

where the expressions of the $C_{k,n-k}^{pq}$ Taylor series expansion coefficients are reported in [11]. Note that $\langle |S_{hv}|^2 \rangle_{\delta,a,b} = \langle |S_{vh}|^2 \rangle_{\delta,a,b}$ and $\langle S_{vv} S_{hh}^* \rangle_{\delta,a,b} = \langle S_{hh} S_{vv}^* \rangle_{\delta,a,b}^*$, whereas the other entries of the covariance matrix are zero in the considered configuration.

We want now to evaluate the PTSM expression of the covariance matrix elements for circular polarization. Therefore, we apply an appropriate change of polarimetric basis [13]. In particular, we are interested in the following diagonal elements of the covariance matrix for circular polarization:
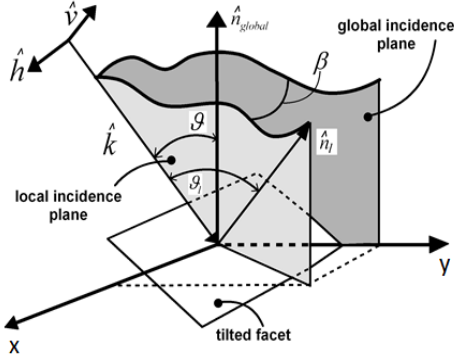
Fig. 1: Geometry of the problem.

$$\begin{cases} 4\langle|S_{RR}|^2\rangle = \langle|S_{hh} - S_{vv} + j2S_{hv}|^2\rangle \\ 4\langle|S_{RL}|^2\rangle = \langle|S_{hh} + S_{vv}|^2\rangle \end{cases} \quad (9)$$

i.e.

$$\begin{cases} 4\langle|S_{RR}|^2\rangle = \langle|S_{hh}|^2\rangle + \langle|S_{vv}|^2\rangle - 2\text{Re}\{\langle S_{hh}S_{vv}^*\rangle\} + 4\langle|S_{hv}|^2\rangle \\ 4\langle|S_{RL}|^2\rangle = \langle|S_{hh}|^2\rangle + \langle|S_{vv}|^2\rangle + 2\text{Re}\{\langle S_{hh}S_{vv}^*\rangle\} \end{cases} \quad (10)$$

where to obtain (10) from (9) the mentioned properties of covariance matrix entries have been exploited. We note also that $\langle|S_{RR}|^2\rangle = \langle|S_{LL}|^2\rangle$. Using (7-8) in (10) we obtain

$$\begin{cases} \langle|S_{RR}|^2\rangle = u_* f_s[|1 - \beta_r|^2 + f_{RR}\sigma^2] \\ \langle|S_{RL}|^2\rangle = u_* f_s[|1 + \beta_r|^2 + f_{RL}\sigma^2] \end{cases} \quad (11)$$

where

$$u_* f_s = \frac{Ak^4 \cos^4\theta}{4\pi^2}|F_V(\theta,\varepsilon)|^2 W(0,2k\sin\theta) = C_{0,0}^{vv} \quad (12)$$

$$\beta_r = \frac{F_H(\theta,\varepsilon)}{F_V(\theta,\varepsilon)} \quad (13)$$

$$f_{RR} = \frac{C_2^{HH}}{f_s} + \frac{C_2^{VV}}{f_s} - 2\frac{\text{Re}\{C_2^{HV}\}}{f_s} \quad (14)$$

$$f_{RL} = \frac{C_2^{HH}}{f_s} + \frac{C_2^{VV}}{f_s} + 2\frac{\text{Re}\{C_2^{HV}\}}{f_s} \quad (15)$$

$$u_* C_2^{PQ} = C_{2,0}^{pq} + C_{0,2}^{pq} \quad (16)$$

The expressions in (11) show that $\langle|S_{RR}|^2\rangle$ depends on the difference between the horizontal and vertical Bragg coefficients and, therefore, the backscattering of the sea surface in this polarization is very low. Conversely, $\langle|S_{RL}|^2\rangle$ is related to the sum of the Bragg coefficients, thus maximizing the return from the sea surface, and minimizing potential double-bounce (more in general, even-bounce) contributions related to the presence of ships. Therefore, we can conclude that RR polarization should be used to maximize the contrast between the ship and the sea background. Finally, note that the expressions obtained in (11) are casted in such a way to highlight the dependence on the large-scale roughness of the sea surface, through the mean

square slope σ^2, and the linear dependence on the friction velocity u_*. Both these quantities can be related to the wind speed at the height of 10 m: the former by using the Katzberg model [14] and the latter by using the relation reported in [8].

3. SIMULATION OF GNSS SCATTERING

In the backscattering configuration the transmitter, the receiver and the backscattering point (on the Earth surface) lie on the same line. Figure 2 shows iso-delay and iso-Doppler lines with the receiver marked in red and the backscattering point marked in green. The delay-Doppler cells are the surface regions inside contiguous iso-delay and iso-Doppler lines. The area of these regions determines the resolution of the system that increases towards the far range from receiver. Figures 3 and 4 show simulation of the overall scattered power in dBW using a TDS-1 acquisition for geometry and satellite positions. Transmitter and receiver are aligned along the same line with the origin of the coordinate system in the backscattering point. The reference system is defined by the *z*-axis normal to the Earth ellipsoid, the *y*-axis in the plane defined by the *z* axis and the vector form origin
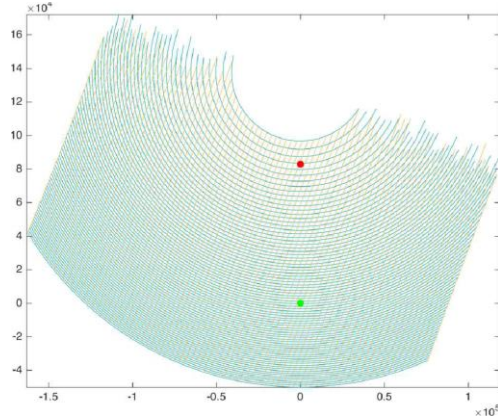

Fig. 2: Iso-delay and iso-Doppler lines. The receiver location is marked in red and the backscattering point is marked in green.
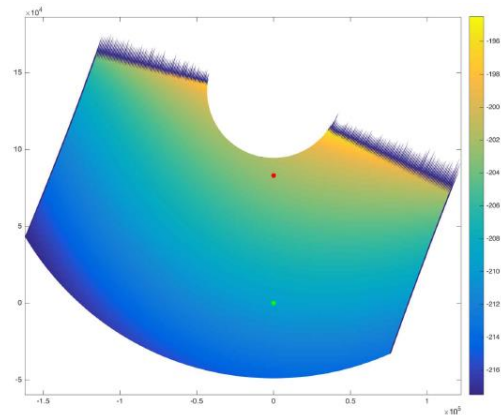

Fig. 3: Overall scattered power in backscattering configuration with Left-Hand Circular receiver antenna polarization (RL polarization).
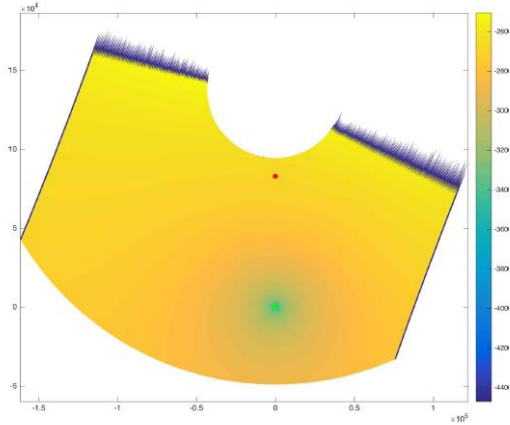
Fig. 4: Overall scattered power in backscattering configuration with Righ-Hand Circular receiver antenna polarization (RR polarization).

to receiver (global incidence plane, see Fig. 1) and the *x*-axis orthogonal to both. TDS-1 acquisition is on June, 20, 2015, 06 hours, Track 62 acquisition 44 with GPS space vehicle 62. The incidence angle is 7.3 degrees, so that KAGO is dominant at this small angle. However, results clearly show that in this configuration the received sea-scattered signal is much weaker than in the forward scattering case, and that at RR polarization it is particularly weak. By using the PTSM model developed here, we can verify (see Fig. 5) that this is true also at higher incidence angles, for which the GNSS backscattered signal is dominated by the Bragg scattering component.

4. REFERENCES

[1] M. P. Clarizia and C. S. Ruf, "Wind speed retrieval algorithm for the cyclone global navigation satellite system (cygnss) mission," *IEEE Transactions on Geoscience and Remote Sensing*, vol. 54, no. 8, pp. 4419–4432, Aug. 2016.

[2] G. Foti, C. Gommenginger, P. Jales, M. Unwin, A. Shaw, Robertson C., and J. Rosell, "Spaceborne gnss reflectometry for ocean winds: First results from the uk techdemosat-1 mission," *Geophysical Research Letters*, vol. 42, no. 13, pp. 5435–5441, 2015.

[3] M. P. Clarizia, P. Braca, C. S. Ruf, and P.Willett, "Target detection using GPS signals of opportunity*," Proceedings of 18th IEEE International Conference on Information Fusion (Fusion)*, pp. 1429–1436, July 2015.

[4] S. L. Ullo, G. Giangregorio, M. di Bisceglie, C. Galdi, M. P. Clarizia, and P. Addabbo, "Analysis of gps signals backscattered from a target on the sea surface," in *2017 IEEE International Geoscience and Remote Sensing Symposium (IGARSS)*, July 2017, pp. 2062–2065.

[5] A. Di Simone, L. M. Millefiori, G. Di Martino, A. Iodice, D. Riccio, G. Ruello, P. Braca, and P. Willett, "Spaceborne gnss-reflectometry for ship detection applications: impact of acquisition geometry and polarization," in *2018 IEEE International Geoscience and Remote Sensing Symposium (IGARSS)*, submitted.

[6] A. Di Simone, H. Park, D. Riccio, and A. Camps, "Sea target detection using spaceborne gnss-r delay-doppler maps: Theory and experimental proof of concept using tds-1 data," *IEEE Journal of Selected Topics in Applied Earth Observations and Remote Sensing*, vol. 10, no. 9, pp. 4237–4255, Sept 2017.

[7] V. U. Zavorotny, A. G. Voronovich, "Two-Scale Model and Ocean Radar Doppler Spectra at Moderate- and Low-Grazing Angles", *IEEE Trans. Antennas Propagat.*, vol. 46, no. 1, pp. 84–92, 1998.

[8] T. Elfouhaily, B. Chapron, and K. Katsaros, "A Unified Directional Spectrum for Long and Short Wind-Driven Waves," *J. Geophys. Res.*, vol. 102, no. C7, pp. 15781–15796, 1997.

[9] F. T. Ulaby, R. K. Moore, and A. K. Fung, *Microwave Remote Sensing: Active and Passive*, Addison-Wesley, Reading, MA, USA, 1982.

[10] A. W. Bjerkaas and F. W. Riedel, "Proposed model for the elevation spectrum of a wind-roughned sea surface," *Tech. Rep. APL-TG-1328-I-31*, Appl. Phys. Lab., John Hopkins Univ., 1979.

[11] A. Iodice, A. Natale, and D. Riccio, "Retrieval of Soil Surface Parameters via a Polarimetric Two-Scale Model," *IEEE Trans. Geosci. Remote Sens.*, vol. 49, no. 7, pp. 2531–2547, 2011.

[12] G. Di Martino, A. Iodice, A. Natale, and D. Riccio, "Polarimetric Two-Scale Two-Component Model for the Retrieval of Soil Moisture Under Moderate Vegetation via L-Band SAR Data," *IEEE Trans. Geosci. Remote Sens.*, vol. 54, no. 4, pp. 2470–2491, 2016.

[13] J. S. Lee and E. Pottier, *Polarimetric Radar Imaging: From Basics to Applications*, CRC Press, Boca Raton, FL, USA, 2009.

[14] S. J. Katzberg, O. Torres, and G. Ganoe, "Calibration of reflected GPS for tropical storm wind speed retrievals", *Geophysical Research Letters*, vol. 33, L18602, 2006.
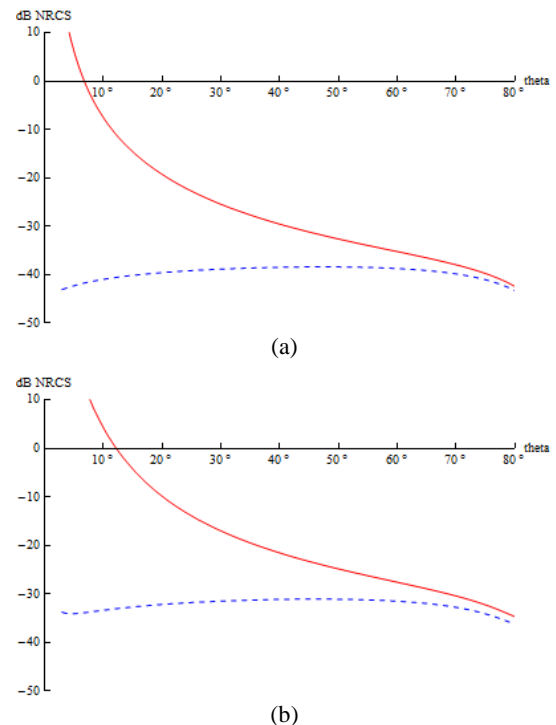
(a)

(b)

Fig. 5: Sea backscattering NRCS as a function of the incidence angle for GPS L1 incident field, and for RL (red solid line) and RR (blue dashed line) polarizations. Wind speed: 2 m/s (a), 20 m/s (b).